GT2023-104038

EXPERIMENTAL STUDY OF COMPRESSIBLE FILM COOLING SCALING AND HOLE GEOMETRY

Dale W. Fox^{1,*}, Michael Furgeson¹, Elise M. Flachs¹, and David G. Bogard¹

¹The University of Texas at Austin Walker Department of Mechanical Engineering Austin, TX, USA

ABSTRACT

While modern gas turbine engines operate at hot gas path velocities approaching the speed of sound, few facilities have studied the effects that the flow's compressibility can have on the adiabatic effectiveness. A new facility at the University of Texas at Austin has been developed to investigate these high Mach number effects and how to appropriately scale laboratory film cooling experiments to engine conditions. This study investigates two film cooling hole geometries, a baseline 7-7-7 shaped film cooling hole and a recent design which has been numerically optimized for increased effectiveness. Both holes are tested at mainstream Mach numbers of 0.25 and 0.50 in a flat plate test section. The optimized hole outperforms the effectiveness of the baseline geometry at all blowing ratios tested, matching the trend in the results of previous studies on these geometries. However, there is a marked decrease in film cooling hole performance as the Mach number is increased.

Keywords: film cooling, shaped holes, transonic, compressible, Mach number, heat transfer, fluid mechanics, experimental, gas turbine engines

NOMENCLATURE

Roman letters

AO Adjoint Optimization C_d Discharge Coefficient d Metering Hole Diameter EDM Electro-discharge Machining

L Hole length

LES Large Eddy Simulation

P Pitch

PLA Polylactic Acid Plastic

r Recovery Factor

SI Sharp Inlet

SLA Stereolithography

Greek Alphabet

 η Adiabatic Effectiveness γ Specific Heat Capacity Ratio

Dimensionless Groups

 \mathcal{M} Blowing Ratio \mathcal{D} Density Ratio Ma Mach Number \mathcal{P} Pressure Ratio Re Reynolds Number \mathcal{T} Temperature Ratio \mathcal{V} Velocity Ratio

Superscripts and Subscripts

Area-Averaged

Mainstream

No film

aw

Adiabatic wall

Coolant

r Recovery Stagnation

INTRODUCTION

Gas turbine engines are used extensively in propulsion and energy generation. As such, gas turbines are indispensable in our daily lives, and much research has been conducted to increase their power output without compromising component longevity. Thermodynamics inform us that higher gas temperatures at the turbine section inlet yield a higher work output. However, inlet gas temperatures and cooling effectiveness are limited by the material properties of turbine airfoils. Air expelled from the combustor exceeds the melting point of the airfoils, requiring the need for active cooling technology [1]. Modern turbine engine airfoils feature internal cooling passages in which cool air absorbs heat along the length of the component. In addition, small holes allow a portion of the cool air to pass through the airfoil and provide a thin layer of protection against the mainstream gas. Many parameters affect the performance of these film cooling

^{*}Corresponding author: dale.fox@solarturbines.com

holes. Literature supports the strong dependence film cooling effectiveness has on blowing ratio, velocity ratio, and temperature ratio between the coolant and mainstream gas. Interestingly, compressibility effects have largely been neglected for shaped film cooling holes, with most film cooling testing occurring at mainstream Mach numbers well below the speed of sound.

Historically, hole geometry was limited by the manufacturing methods, whether it be laser drilling cylindrical holes or creating expansion holes via electrodischarge machining (EDM) [1]. The development of additive manufacturing (AM) offers more flexibility in the optimization of film cooling hole design, and opportunities exist to substantially improve film cooling performance through CFD solvers, such as the adjoint optimization technique implemented by Jones *et al.* [2].

Studies on Compressible Film Cooling

Very few experimental studies have been conducted to evaluate Mach number effects due to the inherent difficulty of performing high speed tests. Cylindrical hole experiments performed by Liess [3] over a range of mainstream Mach numbers from $Ma_{\infty}=0.3$ to 0.9 at a blowing ratio of $\mathcal{M}=0.4$ showed no significant effects due to varying Mach number. Their conclusion that "Mach number in the mainstream has no measurable effect on film cooling parameters" was the basis for justifying the enormous subsequent studies done with low speed facilities. More recently, experiments by Zhou *et al.* [4] also demonstrated that the performance of cylindrical holes is not significantly affected by changes in mainstream Mach number for a range of $Ma_{\infty}=0.07$ to 0.70 and $\mathcal{M}=0.40$ to 1.25.

Two studies from Karlsruhe Institute of Technology by Gritsch et al. [5] and Saumweber and Schulz [6] explored Mach number effects on film effectiveness for cylindrical and shaped hole geometries. The Gritsch et al. [5] study used cylindrical, fan shaped, and laid-back fan shaped holes with mainstream Mach numbers of $Ma_{\infty} = 0.3$, 0.6, and 1.2. The authors noted that for the $Ma_{\infty} = 1.2$ case, a bow shock was generated upstream of the coolant and ultimately forces the coolant jet toward the wall. For the shaped holes at $Ma_{\infty} = 0.6$, Gritsch *et al.* [5] found that the higher pressure ratio, necessary for the higher Mach number holding Re constant, induced non-uniform coolant distribution; coolant was either ejected at the hole centerline or was skewed to one side of the hole. The non-uniformity of coolant distribution across the surface contributed to a significant decrease in film effectiveness for fan shaped holes for $Ma_{\infty} = 0.3$ to 0.6 with $M \ge 1.0$. Contrastly, an increase in film effectiveness was observed for the laid-back fan shaped hole geometry.

In a more recent study, Saumweber and Schultz [6] investigated a fan shaped hole that was similar to the previous study [5]. At lower blowing ratios, $\mathcal{M} < 1.5$, or lower Mach numbers, $Ma_{\infty} < 0.3$, they found a slight improvement of film effectiveness with increasing Mach number which they attributed to a thinner approach boundary layer. However, there was more than 50% degradation of adiabatic effectiveness when the Mach number increased from 0.3 to 0.45 with a high blowing ratio of $\mathcal{M} = 2.5$. The dramatic decrease in adiabatic effectiveness was found to be due to the coolant jet becoming biased to one side of the coolant hole exit, and hence having a narrower distribution of coolant.

This asymmetry was attributed to in-hole separation from the sidewall due to "increased pressure ratio at high Mach number".

A particularly significant computational study performed by Oliver *et al.* [7] supports the existence of Mach effects in shaped film cooling holes. Through a Large Eddy Simulation (LES), a substantial decrease in adiabatic effectiveness was found for the $Ma_{\infty}=0.50$ compared to $Ma_{\infty}=0.25$ when all other parameters were held constant. The generation of shock waves, evident from the centerline contours, induced coolant biasing within the diffuser section of the hole and caused poor coolant distribution downstream of the hole exit.

Thus, investigating adiabatic effectiveness at engine realistic Mach numbers is paramount in characterizing the performance of shaped film cooling holes. To characterize the effect of Mach number on film cooling performance, the Turbulence and Turbine Cooling Research Laboratory (TTCRL) at the University of Texas at Austin has finished construction of a new wind tunnel capable of sustaining mainstream velocity in the compressible regime. A thorough description of this new facility is presented in subsequent sections.

Present Study

The present study experimentally evaluates the compressibility effect on adiabatic effectiveness for two hole geometries. These two geometries are the crossflow adjoint optimized hole (AOpt) developed by Jones *et al.* [2], and the standard laidback fan-shaped hole, 7-7-7 SI [8]. The thermal contours were measured for mainstream Mach numbers $Ma_{\infty}=0.25$ and $Ma_{\infty}=0.50$ at varying blowing ratios. The adiabatic effectiveness, η_r , is defined based on the recovery temperature T_{∞}^r , adiabatic wall temperature T_{aw} , and the coolant recovery temperature T_c^r , as shown in Equation 1.

$$\eta_r = \frac{T_{\infty}^r - T_{aw}}{T_{\infty}^r - T_C^r} \tag{1}$$

This definition was employed in accordance with the observations made in a companion paper by Fox *et al.* [9], which demonstrates that the mainstream and coolant recovery temperatures may be approximated by

$$T^{r} = T^{\circ} \frac{\left(1 + \frac{\gamma - 1}{2} r M a^{2}\right)}{\left(1 + \frac{\gamma - 1}{2} M a^{2}\right)} \tag{2}$$

Recognize that as $Ma_{\infty} \to 0$, $T^r \to T^o \approx T$. As such when $Ma_{\infty} \to 0$, as in low speed studies, $\eta_r \approx \eta$. While measurement of Ma_{∞} is straightforward, the value of Ma_c is less clear. Interpretation of this parameter is described in further detail in [9]. Also note that for this study the recovery factor is treated as $r = 0.89 = Pr^{1/3}$, following the approximation for a flat plate, turbulent boundary layer [10].

This all considered, the primary goal for this study was to determine effects of relatively high mainstream Mach number on the film cooling performance of the two hole geometries. In addition, how the performance of the two geometries compare is discussed. Studies performed at low mainstream Mach number found that the AOpt hole performs significantly better than the 7-7-7 SI hole, when evaluated under the same conditions [2, 11, 12].

It is of interest to determine whether this augmented performance is maintained at higher mainstream Mach number.

TEST FACILITIES AND EXPERIMENTAL METHODS

In order to experimentally study the effects of high mainstream Mach number, a new wind tunnel facility was developed. This wind tunnel was originally proposed to expand upon the LES results of Oliver *et al.*[7], which predicted increasing Ma_{∞} reduces the performance of a standard shaped hole.

Overview of Wind Tunnel and Coolant System

A schematic of the newly constructed wind tunnel can be viewed in Figure 1. It is a closed loop, recirculating wind tunnel with several interrelated components to ensure accurate and repeatable data acquisition at high speed. The mainstream blower in the lower left corner of the figure supplies the pressure to drive the mainstream flow into the test section. The wind tunnel is constructed with two separate test sections, one designed for simplified flat plate measurements and one with a two-passage linear cascade for blade and vane studies. The flat plate test section is the focus of the present study. The mainstream air travels through twelve inch schedule 80 CPVC to the settling chambers, where a diffuser slows the flow down prior to reaching mainstream heat exchangers.

Cooling coils within the heat exchangers are fed from the facility's local chilled water supply. This water flow rate can be set to regulate mainstream temperature across varying mainstream Mach number. Also included in the design of the cooling coils are flow conditioning screens that assist in the breakup of large turbulent eddies created by the coils. The flow continues for several feet in the settling chamber to allow the turbulence to decay, before proceeding through a nozzle into the test section.

The secondary flow loops consist of several sub-assemblies that condition and prepare air for use as coolant in the film cooling studies. Air is continuously brought into the tunnel using the pressurization blower and passed through the desiccant tanks, which ensure the humidity within the tunnel is near zero. Maintaining a low humidity is essential in film cooling studies since the liquid nitrogen cooled air would freeze any residual moisture in the air and plug film cooling holes and other small flow paths within the tunnel.

The coolant heat exchanger and nitrogen dewars allow the coolant to be chilled to appropriate temperatures during the film cooling experiment. This air is driven through the heat exchanger and into the coolant supply plenum by the coolant blower, for which the speed is controlled by variable frequency drive (VFD).

The mainstream speed is also set by VFD. The speed is measured by a pitot-static probe, which also has an embedded thermocouple for measuring stagnation temperature. The coolant stagnation temperature is measured through a thermocouple within the coolant plenum, where the velocity of the coolant is slow enough that a static temperature measurement is equal to the stagnation temperature within uncertainty. Similarly, the coolant static pressure is measured via a pressure transducer within the plenum, and this measurement is used in determining the pressure ratio \mathfrak{P} .

Hole Geometries

Two hole geometries were investigated in the present study, a sharp inlet 7-7-7 hole, and a novel adjoint optimized (AOpt) hole developed by Jones et al. [2]. The 7-7-7 SI hole dimensions are set by the specifications made by Shroeder and Thole [8]. Specifically, the geometry has a 7° forward and lateral expansion in the diffuser section with an overall length from the inlet to exit plane of L/d = 6, and metering section length of 2.5d. Both the 7-7-7 SI and AOpt hole geometries have an inclination angle of 30°. For the AOpt hole, called X-AOpt in previous studies, geometry was optimized based off an initial geometry of a 15-15-1 SI hole under a steady crossflow coolant feed with a coolant channel inlet velocity ratio of $V_c = 0.2$ and a velocity ratio of $\mathcal{V} = 1.67$. The protrusions on the outer surface, as depicted in Fig. 2, generate a counter-rotating vortex pair that pushes coolant closer to the surface delaying jet separation. Although originally developed for cross flow, previous studies performed in co-flow [11, 12] and plenum fed [2] configurations found that this hole performed significantly better than other geometries, including the 7-7-7 SI.

For the present study, the hole geometries were constructed at engine scale using a Formlabs stereolithography (SLA) printer, in the form of a test coupon with a row of six holes. After being manufactured, these test coupons were painted black to provide a uniform wall emissivity of approximately unity. As such, biasing of the IR image from reflected radiation is minimized. SLA was chosen as it demonstrates very good dimensional tolerancing, at a cited value of $\pm 0.2\%$ with a lower limit of ± 0.1 mm [13]. The holes were constructed with supports at a 30° angle such that the metering hole axis was perpendicular to the print bed, and the mainstream surface was facing away from the print bed. The material resin chosen was Formlabs standard, clear resin with a layer height of 0.025mm. Unfortunately, this material is a proprietary photopolymer, and thermal conductivity data is not currently available. Future work will investigate the exact thermal properties of this material in greater detail. Both holes have a metering hole diameter of d = 1.1 mm and a pitch of P = 6mm, or P/d = 5.5. These primary dimensions were verified by measurement of manufactured parts, as shown in Figure 3. This figure also demonstrates good feature resolution of the prints and minimal roughness. Note that some observed roughness in the midplane image is artificial, due to the machining processes used to cut the coupon at the centerline, to create the image. Before testing, all holes were carefully examined and no defects could be observed by eye. While there is a slight chip observed at the hole outlet in the second image of Figure 3c, this was artificially created as a result of mishandling after the first image. The two images in Figure 3c are of the same mid-plane, but taken at different times.

Test Conditions

In this set of experiments, the test section was held at approximately constant mainstream stagnation pressure and temperature while the mainstream Mach number was changed, between $Ma_{\infty} = 0.25$ and $Ma_{\infty} = 0.50$. The recorded properties of the mainstream and coolant gas streams for both holes are shown in Table 1. In addition to mainstream Mach number and main-

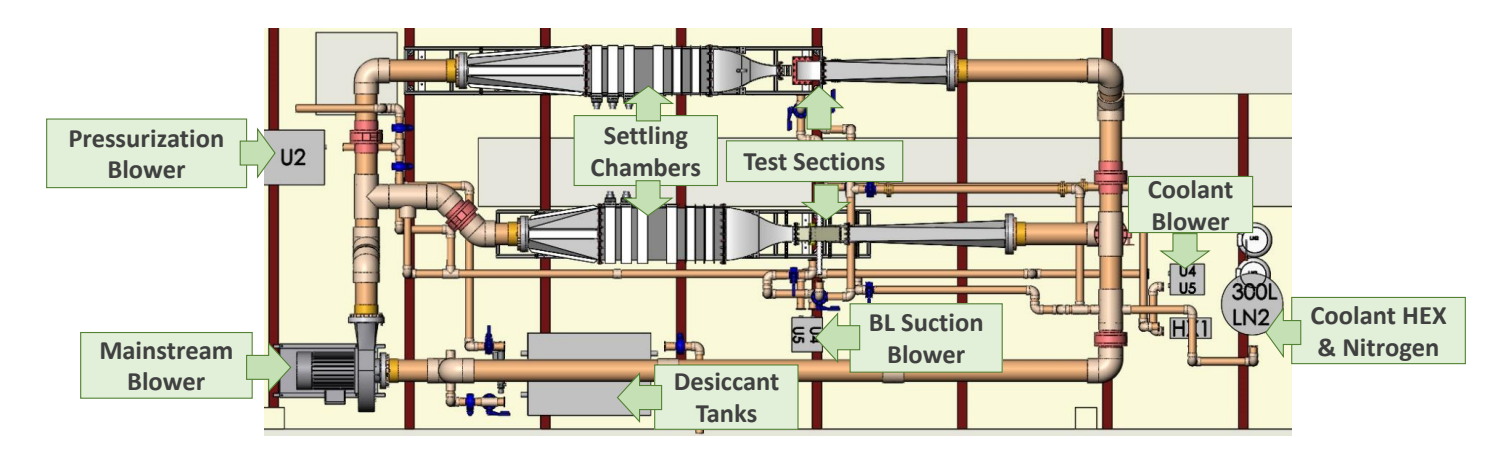


FIGURE 1: SCHEMATIC OF THE TTCRL HIGH-SPEED WIND TUNNEL FOR FILM COOLING STUDIES

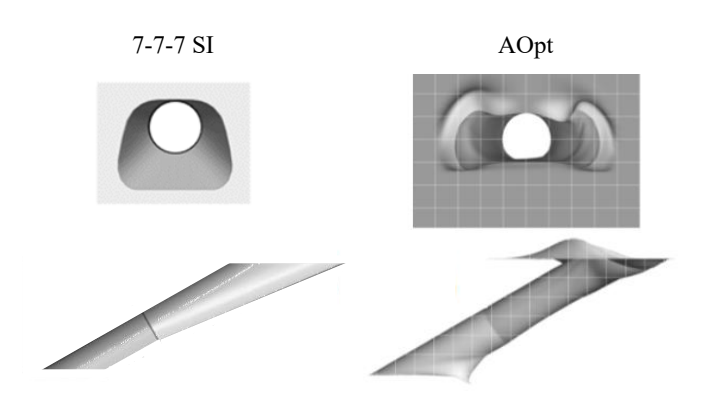


FIGURE 2: BASIC DESIGN OF THE TWO HOLE GEOMETRIES USED IN THIS STUDY

stream hole Reynolds number Re_d , the table reports stagnation temperature ratio \mathcal{T}^o , static pressure ratio \mathcal{P} , and blowing ratio \mathcal{M} . Note that the aforementioned scaling parameters are all defined as ratios of coolant to mainstream value. Since the mainstream stagnation temperatures and pressures remained constant while the velocity changed, Re_d necessarily changed.

Due to current limitations in mainstream temperature regulation, mainstream stagnation temperature was $T_{\infty}^o = 315 \, \mathrm{K}$ at $Ma_{\infty} = 0.50$, and $T_{\infty}^o = 307 \, \mathrm{K}$ at $Ma_{\infty} = 0.25$. At $\mathfrak{T}^\circ = 0.83$, the corresponding coolant stagnation temperatures were $T_c^o = 263 \, \mathrm{K}$ and $T_c^o = 256 \, \mathrm{K}$, respectively. For this study, $\mathfrak{T}^\circ = 0.83$ was chosen for consistency with previous studies performed at TTCRL such as [11, 12]. At present, the mainstream flow has not been characterized, and a turbulence generation grid has not yet been implemented to replicate engine conditions. However, the authors recognize the importance of such measurements and improvements prior to further studies.

Experimental Methods

In these experiments, the flowrate of air through the film cooling holes is estimated, not directly measured. To do so, the standard 7-7-7 film cooling holes are assumed to have a discharge coefficient $C_d = 0.8$, and the AOpt holes are assumed to have $C_d = 1.2$ from the results of Gutierrez *et al.* [11]. Note that $C_d > 0.8$

TABLE 1: FLOW PARAMETERS FOR MACH VARIATION

			= CT	14 0	25		
	7-7-7 SI			$Ma_{\infty} = 0.25$			
Re_d	5,960	5,920	6,060	5,890	5,870	5,880	
\mathfrak{M}	0.61	1.03	1.49	2.05	2.59	3.09	
\mathcal{P}	1.02	1.06	1.12	1.23	1.37	1.54	
\mathfrak{T}°	0.84	0.83	0.83	0.82	0.81	0.82	
	7-7-7 SI $Ma_{\infty} = 0.50$						
Re_d	11,250	11,200	11, 120	11,070	11,050	10,950	
\mathfrak{M}	0.54	0.64	1.06	1.31	1.60	1.83	
\mathcal{P}	1.06	1.09	1.24	1.37	1.56	1.74	
\mathfrak{T}°	0.82	0.82	0.81	0.82	0.81	0.81	
	AOpt $Ma_{\infty} = 0.25$						
Re_d	6,300	6,380	6,420	6,380	6,370	6,350	
\mathfrak{M}	0.90	1.07	1.48	1.93	2.43	2.92	
\mathcal{P}	1.02	1.03	1.06	1.10	1.16	1.23	
\mathfrak{T}°	0.84	0.84	0.83	0.84	0.83	0.82	
	$\mathbf{AOpt} \qquad Ma_{\infty} = 0.50$						
Re_d	10,950	10,920	11,030	10,830	10,860	10,770	
\mathfrak{M}	0.71	1.03	1.51	2.06	2.53	2.85	
\mathcal{P}	1.05	1.11	1.24	1.45	1.68	1.86	
\mathfrak{T}°	0.83	0.83	0.84	0.83	0.82	0.81	

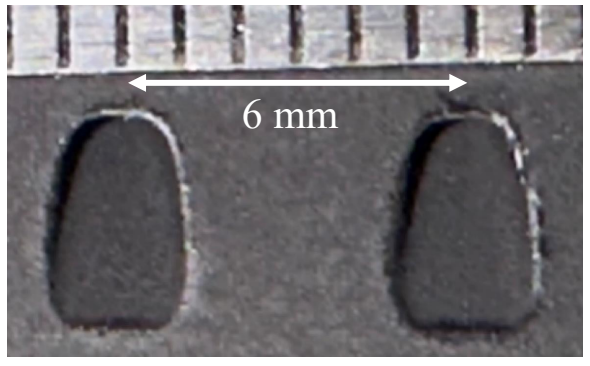
1 is achievable for the AOpt hole as C_d is traditionally calculated using the area of the metering hole [14]. As the diffuser of the AOpt hole is highly effective, pressure recovery from the metering hole to the hole exit is significant. With these assumed C_d values, blowing ratio is calculated using the following equation:

$$\mathcal{M} = \frac{C_d \mathcal{T}^{\circ} \mathcal{P}^{\frac{\gamma - 1}{2\gamma}}}{M a_{\infty}} \sqrt{\frac{2}{\gamma - 1} \left(\mathcal{P}^{\frac{\gamma - 1}{\gamma}} - 1\right)}$$
(3)

where pressure ratio, stagnation temperature ratio, and mainstream Mach number are measured. Equation 3 is derivable through rearrangement of the discharge coefficient equation for film cooling in compressible flow [14] and the definitions of pressure ratio, temperature ratio, blowing ratio, and Mach number.

While under ideal circumstances blowing ratio would be determined by direct measurement of mass flow rate, this form of

(a) 7-7-7 Hole Outlet



(c) 7-7-7 Hole Midplane



(b) AOpt Hole Outlet

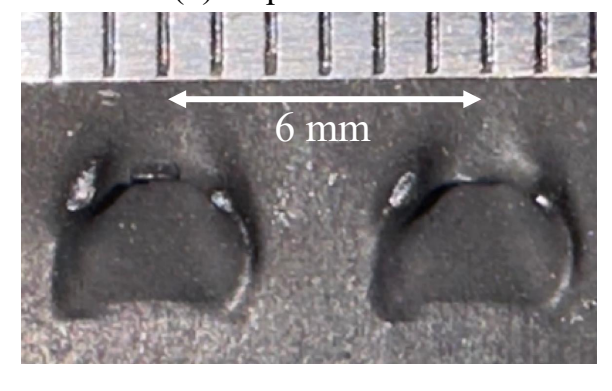




FIGURE 3: IMAGES OF THE HOLE OUTLETS OF THE 7-7-7 SI COUPON (A) AND AOPT COUPON (B), AS WELL AS MIDPLANE IMAGES OF THE 7-7-7 SI (C).

blowing ratio was necessitated by the failure of the intended process for doing so. Extensive testing of the orifice meters setup in the commissioning of the wind tunnel showed an extreme sensitivity in the flow meters to variables that could not be determined.

Infrared thermography is used for all surface temperature measurements, where a measurement area of $-5 \le x/d \le 20$ and $-11 \le z/d \le 11$ was recorded in this study. This range of z/d captures the center 4 film cooling holes, with the 5th and 6th holes being adjacent to either end of the measurement area. A FLIR A655sc camera is used to capture the images through a broadband anti-reflective (BBAR) zinc-selenide window. To ensure the accuracy of the thermal measurements, the IR camera was calibrated in-situ with a specialized calibration coupon. This coupon uses a slot instead of discrete film cooling holes and has thermocouples mounted on copper plates embedded in the surface. The copper plate and slot are to aid in the uniformity of temperature over the calibration viewing area. As with the test coupons, the calibration coupon and associated copper plates were painted black to provide a uniform emmisivity of approximately unity. An example of the resulting calibration curve for the signal from the camera is shown in Figure 4.

A conduction correction was performed on the data taken in this study, using the same method of 1-D correction presented in [12], but with the recovery form η_0^r .

$$\eta_r = \frac{\eta_{uncorrected} - \eta_0^r}{1 - \eta_0^r} \tag{4}$$

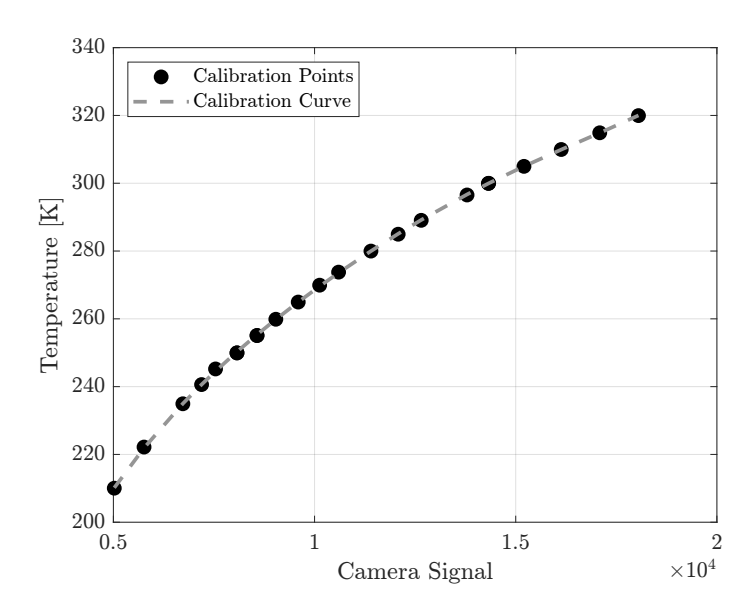


FIGURE 4: TYPICAL IN-SITU CALIBRATION CURVE OF THE IR CAMERA

Their low speed facility measured an η_0 used for correcting the effectiveness by blocking the central film cooling holes and matching the blowing ratio, measuring the effectiveness in the space where there are no longer film cooling jets being produced while preserving the same backside convective boundary condition as in an normal film cooling experiment. However, due to the dif-

ficulty of blocking the high pressure film cooling holes in this study, η_0^r was instead taken from an area adjacent to the measurement area where film cooling is absent, but still visible by the IR camera.

To create a robust correction using this simplified method, the data was imported and corrected in such a manner that η_0^r values are specific to each set point; i.e. for some M and Ma_{∞} at a given setpoint, the data is imported for that setpoint, η_0^r is recorded for that setpoint at an area adjacent to the film cooling holes, and Equation 4 is applied for that setpoint. In addition, the correction accounted for streamwise variations in η_0^r by correction with a laterally averaged version of η_0^r . i.e for every x/d and every setpoint, there is a unique η_0^r which is applied with Equation 4. This lateral average is applied over the adjacent region selected, which again is outside the film cooling jets. A final component of the correction was the consideration of spanwise variation in η_0^r . While not intentional, the present study observed a spanwise temperature gradient in the test section. This was compensated in η_0^r by applying the same aforementioned method, but averaging an adjacent region both above (z/d > 16.5) and below (z/d < -16.5) the row of film cooling holes. To demonstrate this discrepancy and to help explain how it was corrected, Figure 5 shows $\bar{\eta}_0^r$ for each blowing ratio, at each mainstream Mach number for both this "top correction" (TC) and this "bottom correction" (BC). Here it may be observed that the variation in $\bar{\eta}_0^r$ is minimal with varying \mathcal{M} , but that variation exists in the spanwise direction. Although not shown for brevity, the data also showed that $\bar{\eta}_0^r$ had minimal dependence on x/d.

A demonstration of the conduction correction in practice is shown in Figure 6, where the difference in effectiveness outside the region of the film cooling holes is clear. This being stated, it is recognized the the correction is imperfect as these values are not zero. Notably, lateral conduction has a large effect near the film cooling holes, which is not considered in a 1-D correction. However, the bias from this imperfect correction is consistent among the high speed cases presented, making their comparison valid.

Experimental Uncertainties

The uncertainty associated with calibrated instrumentation is described using both bias and precision uncertainty. Individual measurements have been propagated forward through the calculations by the sequential perturbation method described in Moffat [15]. The perturbation method determines the final bias and precision uncertainty in the non-dimensional parameters and adiabatic effectiveness.

Representative combined bias uncertainties of Ma_{∞} , Re_d , \mathcal{P} , and \mathcal{T}^o are shown in Table 2 for both Mach number cases, and for low and high \mathcal{M} . These uncertainties are presented as a percentage of the given flow value at that condition. The uncertainty in Mach number is primarily caused by the uncertainty in the static and stagnation pressure measurements. As expected, the relative uncertainty of Mach number for $Ma_{\infty}=0.25$ is larger than that of $Ma_{\infty}=0.50$. δRe_d is consistent across the whole range, and is mostly a function of the uncertainty in temperature which contributes to uncertainty in both density and viscosity. Uncertainty in pressure ratio increases with the magnitude of

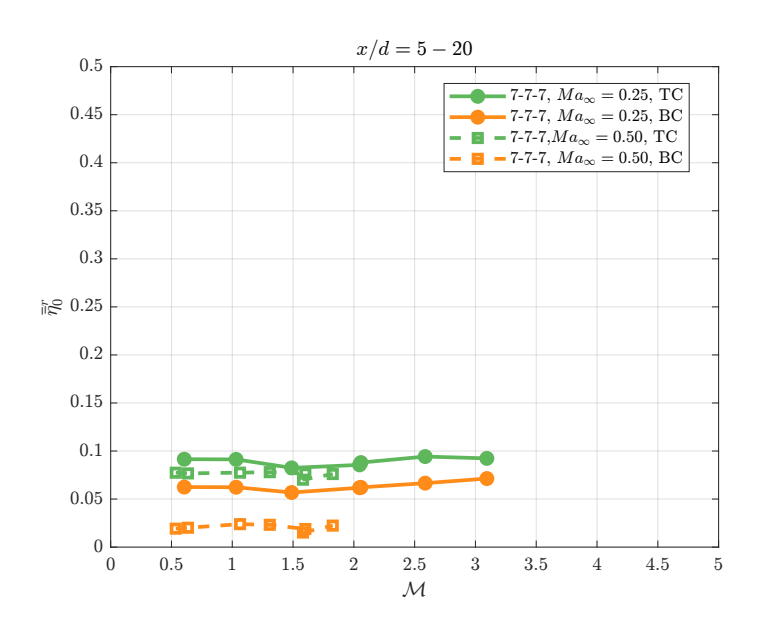


FIGURE 5: η_0^r FOR THE TOP AND BOTTOM REGIONS SELECTED FOR THE CONDUCTION CORRECTION

TABLE 2: RELATIVE BIAS UNCERTAINTY IN FLOW VARIABLES

	Ma_{∞}	= 0.25	$Ma_{\infty} = 0.50$		
Variable	$\mathcal{M} \approx 1$	$\mathcal{M} \approx 2$	$\mathcal{M} \approx 1$	$\mathcal{M} \approx 2$	
$\delta_{Ma_{\infty}}$	1.8%	1.8%	0.50%	0.51%	
δ_{Re_d}	2.0%	2.0%	1.1%	1.1%	
$\delta_{\mathcal{P}}$	2.9%	2.6%	3.1%	2.4%	
$\delta_{\mathfrak{I}^o}$	1.1%	1.1%	1.1%	1.1%	

the pressure ratio, and is driven by the calibration uncertainty of the plenum pressure transducer. This pressure transducer is one of the largest range pressure transducers in the lab, and so has relatively high uncertainty toward the top and bottom of it's range. The temperature ratio uncertainty is clearly a product of the thermocouple uncertainties, and is constant due to the fixed uncertainty of the standard thermocouple calibration.

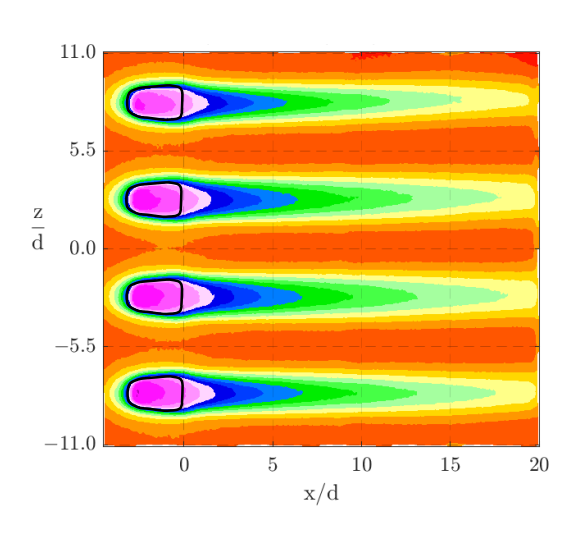
The bias uncertainty of the adiabatic effectiveness varies according to the IR camera calibration, and so is mostly a function of temperature. The bias uncertainty is consistently between 0.030 and 0.035 in η_r . This is actually mostly due to the standard uncertainty used for the thermocouples, with the calibration uncertainty of the camera being a small portion of the overall uncertainty. This value is, in relative terms, approximately 15% of the average η_r value for this case. This relatively high uncertainty can be mitigated by improved in-situ calibration of the thermocouples used for mainstream and coolant temperature measurement.

The precision uncertainty here is determined from statistics on the repetition within a single data point, which in the case of the current experiment is a set of 5 points measured for each blowing ratio setpoint. Representative combined precision uncertainties of these variables are shown in Table 3. The precision uncertainties of all flow variables are generally about an order of magnitude smaller than the corresponding bias uncertainty.

Examining the given uncertainties, it is noteworthy that the

No Conduction Correction

Conduction Corrected



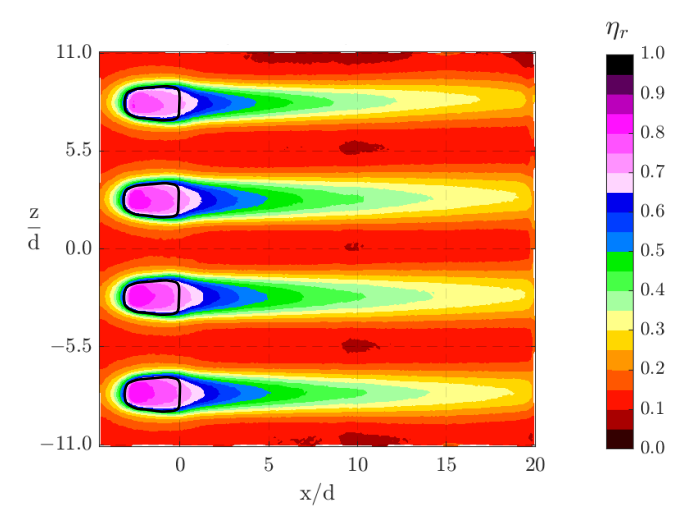


FIGURE 6: THE EFFECT OF CONDUCTION CORRECTION ON TYPICAL FILM COOLING MEASUREMENTS IN THIS STUDY

TABLE 3: RELATIVE PRECISION UNCERTAINTY

	$Ma_{\infty} = 0.25$		$Ma_{\infty} = 0.50$	
Variable	$\mathcal{M} \approx 1$	$\mathcal{M} \approx 2$	$\mathcal{M} \approx 1$	$\mathcal{M} \approx 2$
$\delta_{Ma_{\infty}}$	0.48%	0.87%	0.22%	0.15%
δ_{Re_d}	0.48%	0.88%	0.24%	0.16%
$\delta_{\mathcal{P}}$	0.04%	0.07%	0.08%	0.05%
$\delta_{\mathfrak{I}^o}$	0.04%	0.07%	0.02%	0.01%

uncertainty of $\mathfrak M$ is not presented. Due to the methods used to estimate $\mathfrak M$ in Equation 3, $\delta_{\mathfrak M}$ is difficult to quantify as an assumed C_d is included in the definition. C_d may vary, notably if shockwaves or large seperation regions form within the film cooling hole. This being stated, it is reasonable to say $\delta_{\mathfrak M} \approx f(\delta_{\mathfrak T^o}, \delta_{\mathfrak P}, \delta_{Ma_{\infty}})$, of which the uncertainties are reported in Tables 2 and 3.

The repeatability of measurements must also be considered. While test-to-test repeatability was not established in this study due to time constraints, in-test repeatability was established for all cases by taking a repeat measurement at the end of each experiment. This repeat measurement was taken at $\mathcal{M}\approx 2.00$ for the cases at $Ma_\infty=0.25$ and $\mathcal{M}\approx 1.50$ for the cases at $Ma_\infty=0.50$. The maximum discrepancy between the repeat and original measurements was $\delta_R(\bar{\eta})=0.01$, which will be approximated as the repeatability for this study. This maximum discrepancy occurred for the AOpt hole at $\mathcal{M}\approx 1.50$ and $Ma_\infty=0.50$.

EXPERIMENTAL RESULTS

Area-averaged adiabatic effectiveness, $\overline{\eta_r}$, measurements are presented in Figure 7 for the 7-7-7 SI and AOpt holes over a range of blowing ratios at $Ma_{\infty} = 0.25$ and 0.50. The local η values were averaged across the center four cooling holes over the streamwise range of x/d = 5 to 20. Also presented in Figure 7 are $\overline{\eta_r}$ measurements at $Ma_{\infty} = 0.07$ from a previous study by Gutierrez *et al.* [11]. There are a few items to note when comparing to the

low speed cases from Gutierrez et al. [11]. Test coupons from the lower speed study were constructed using fused deposition (FDM) at roughly 4x larger scale than those of the present study. Therefore, in addition to being conducted in a different low speed facility, the study does not use the exact same coupons as those used in the present study. Furthermore, these low speed cases were performed using a co-flow configuration with a coolant channel outlet velocity ratio $V_c = 0.12$. However, at such low channel velocity the coolant supply is comparable to that of a plenum fed configuration. Indeed, comparing the 7-7-7 results of [11] to that of the plenum fed results from Anderson et al. [16], it may be observed that performance is similar. Regarding hole Reynolds number, $Re_d = 6,200$ for the low speed study [11], which is approximately that of the $Ma_{\infty} = 0.25$ cases used in this study. Furthermore, the present data has a P/d = 5.5 while the low speed data is presented with P/d = 6. Therefore, the high speed data presented in Figure 7 is adjusted to be representative of P/d = 6, such that the comparison is valid. The superposition technique for this adjustment is described by Bogard & Thole [1]. Examining the figure, the AOpt hole trends are similar at $Ma_{\infty} = 0.07$ and $Ma_{\infty} = 0.25$, as expected. Contrarily, there is a significant difference between the performance of the 7-7-7 hole at $Ma_{\infty} = 0.07$ versus the $Ma_{\infty} = 0.25$ case observed in this study. It is notable that the performance is relatively similar at low blowing ratio, before diverging around $\mathcal{M} = 1$. Although a separate study by Saumweber and Schulz [6] notes a slight increase in performance with increasing Ma_{∞} when $Ma_{\infty} < 0.3$, further investigation of performance while varying Ma_{∞} will be required to better understand this difference in performance.

Another notable feature from Figure 7 is that both hole geometries had significantly lower performance at $Ma_{\infty}=0.50$ than at $Ma_{\infty}=0.25$ when examining $\mathfrak{M}>1$. For the 7-7-7 geometry, there is a steep decline in performance such that $\overline{\eta}_r$ at $\mathfrak{M}=1.83$ is approximately the same as that for $\mathfrak{M}=0.54$. Examining peak effectiveness of the AOpt hole, $\overline{\eta}_r$ for the AOpt hole declined from 0.31 for $Ma_{\infty}=0.25$ to just 0.25 for $Ma_{\infty}=0.50$.

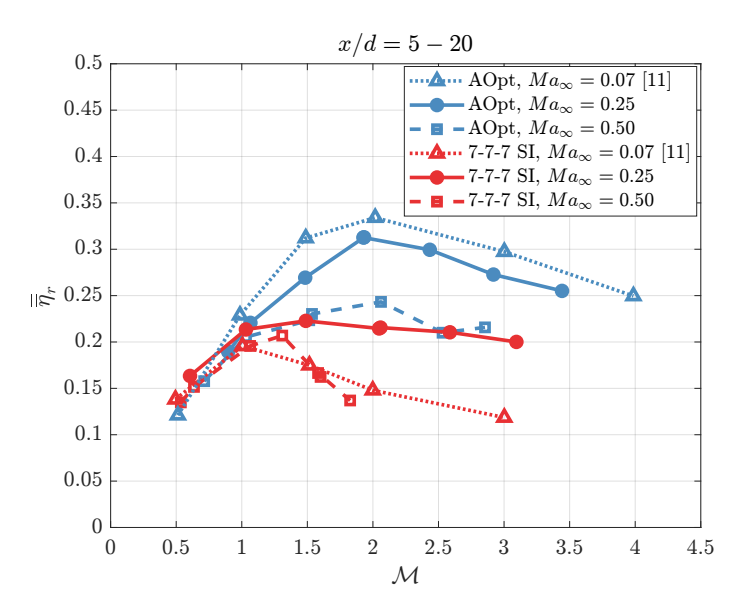


FIGURE 7: AREA-AVERAGED η_r FOR x/d=5-20 WITH VARYING $\mathfrak{M},$ HOLE GEOMETRY AND MACH NUMBER

Comparing the two hole geometries at the same Ma_{∞} , for all $\mathcal{M}>1$ the AOpt hole geometry performed remarkably better than the 7-7-7 hole geometry. However, it is noteworthy that the decline in performance for the AOpt hole at $Ma_{\infty}=0.50$ causes it to perform similarly to the 7-7-7 hole at $Ma_{\infty}=0.25$. Below a blowing ratio of unity, the holes perform similarly at all mainstream Mach numbers.

Contours of η_r for the 7-7-7 holes are presented in Figure 8 for $Ma_{\infty} = 0.25$ (top three images) and $Ma_{\infty} = 0.50$ (bottom three images). The blowing ratios for each case are denoted in the top right-hand corner of each image and range from approximately $\mathcal{M} = 0.60$ to $\mathcal{M} = 2.00$. While the η_r distributions are similar between the two Mach numbers for \mathcal{M} < 1, at the highest blowing ratio presented there are significant differences. The jet profile at the exit of the film cooling hole narrows for $Ma_{\infty} = 0.50$, $\mathcal{M} = 1.83$, and predominantly biases to the bottom side of the hole. These changes correspond to the decline in performance observed in Figure 7 and likely are attributed to phenomenon occurring inside the hole at heightened P. Indeed, computational predictions of the companion study by Fox et al. [9] observe supersonic flow and shockwaves within the coolant hole under the condition of $Ma_{\infty} = 0.50$, $\mathcal{M} = 1.75$, $\mathfrak{T}^o = 0.83$, and $Re_d = 10,100$. As the companion study was designed to model the test section of the present study, it is reasonable to expect similar behavior is responsible for the sharp decline in performance seen here. Examining the jet profiles among the 7-7-7 cases, hole to hole uniformity of of the jet profile is good, with some slight deviation observed in the bottom hole for $Ma_{\infty} = 0.50$, $\mathcal{M} = 1.83$.

Contours of η_r for the AOpt cooling holes are shown in Figure 9 for $Ma_\infty=0.25$ and $Ma_\infty=0.50$. The blowing ratios observed for the AOpt holes ranged from approximately $\mathfrak{M}=1.0$ to $\mathfrak{M}=2.5$, notably larger than the 7-7-7 SI cases. This is due to the C_d values for the AOpt holes being significantly larger than that for the 7-7-7 SI holes, resulting in a higher blowing

ratio at the maximum and minimum pressure ratio available. This being stated, the authors note that difficulties in holding the system steady thermally limited the lowest blowing ratio achieved for the AOpt $Ma_{\infty}=0.25$ case. Examining the figure, for the $Ma_{\infty}=0.25$ cases with $M\geq 2$, there is a broader distribution of coolant over the surface resulting in a larger $\overline{\eta_r}$ compared to the corresponding $Ma_{\infty}=0.50$ cases. Focusing on the η_r distributions measured within the coolant holes, it is clear that there is a broader distribution of coolant within the holes for the $Ma_{\infty}=0.25$ cases, which leads to a broader distribution of coolant downstream of the holes. As with the 7-7-7 holes, it is likely that the noticeable decrease in performance is associated with flow phenomenon within the hole.

Unlike the uniform η_r distributions for the 7-7-7 SI cooling holes, the η_r distributions for the AOpt hole feature noticeable biasing of all the coolant jets. Along the row of holes, direction of this biasing is not always consistent, which may leave some gaps in coverage. It is also notable that in some cases the biasing direction would change under the same conditions, as was observed at the $Ma_\infty=0.5$ repeat measurement in this study. For the first measurement the top hole jet was biased upwards, and for the repeat measurement the top hole jet was biased downwards. However, it may be seen in Figure 7, which includes repeat measurements, $\overline{\eta_r}$ was not significantly affected by this change. This is because the the decline in coverage on the side where the jet was biased in the first measurement was compensated by augmented coverage on side where the jet was biased in the repeat measurement.

It is also useful to make a direct comparison of contours from the present work to that of the $Ma_{\infty} = 0.07$ data from Yoon et al. [12]. Yoon et al. [12] was the companion study of Guiterrez et al. [11] and used the same experimental setup. Such a comparison is presented in Figure 10. For the AOpt case, the coolant jets show less jet biasing and a broader distribution of coolant for the $Ma_{\infty} = 0.07$ case, resulting in a higher $\overline{\eta_r}$. At $Ma_{\infty} = 0.25$, the η_r contours within the hole show that the coolant in the hole was much less broadly distributed than that for $Ma_{\infty} = 0.07$. This led to the narrower coolant distribution downstream of the coolant holes and the degradation of cooling performance at higher Mach number. Although biasing varies between the two AOpt cases, it is noteworthy that hole to hole jet non-uniformity exists both in the present study and the low speed study [12]. This would suggest that jet non-uniformity is characteristic of the hole geometry, as the two studies used entirely different test facilities and hole construction methods. Indeed, these differences in construction methods likely also contributed to limitations in the present conduction correction. Effectiveness values outside the film cooling jet are lower for data from the low speed study than for the $Ma_{\infty} = 0.25$ data from this study. Being a solid body, rather than a partially hollow body with a prescribed infill, the test coupons used in this study likely had higher thermal conductivity than those used for the low speed study. In this regard, spanwise and streamwise conduction would be more significant, and thus less well resolved by a 1-D correction.

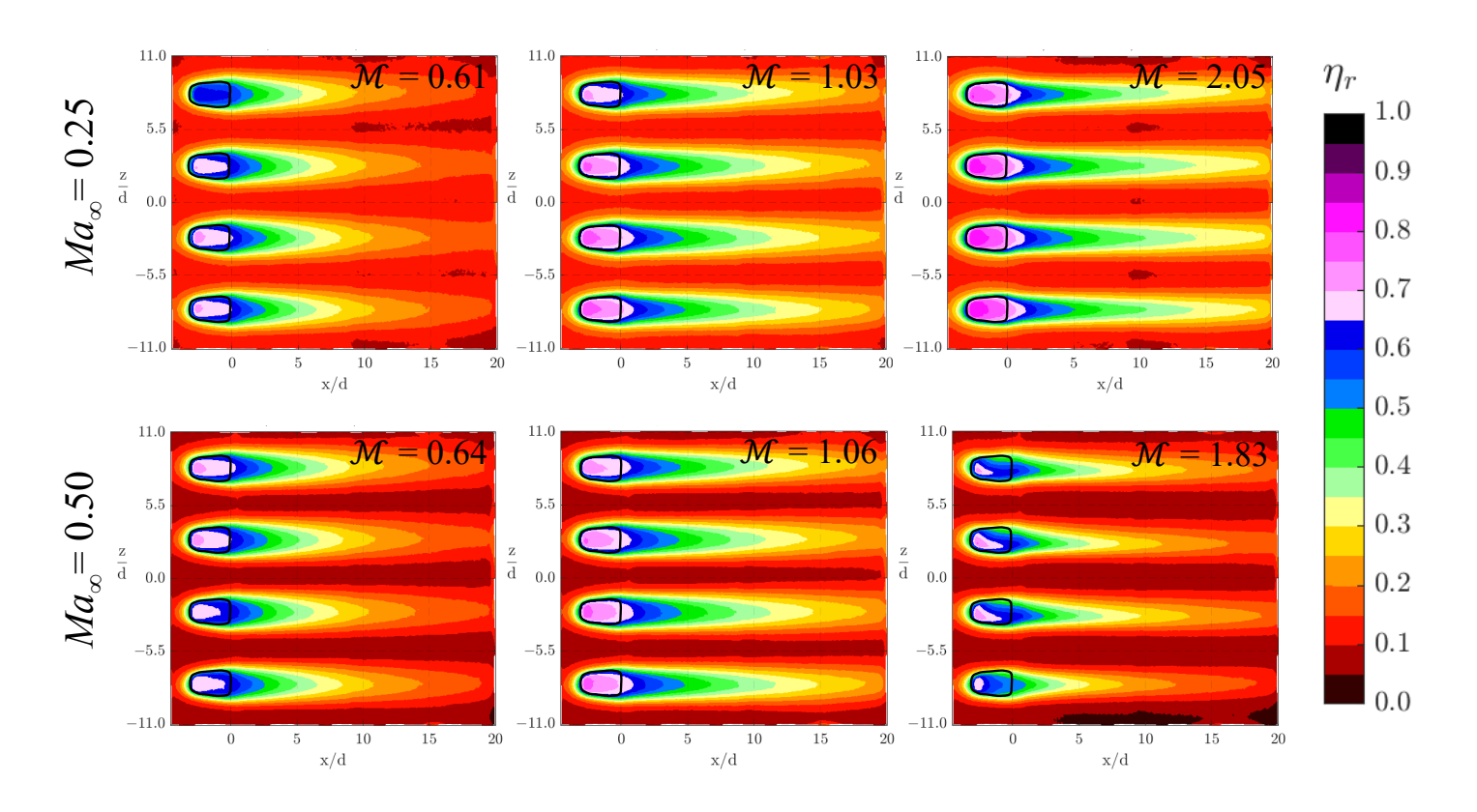


FIGURE 8: 7-7-7 η_r DISTRIBUTION FOR Ma_{∞} = 0.25 AND 0.5, CONDUCTION CORRECTED

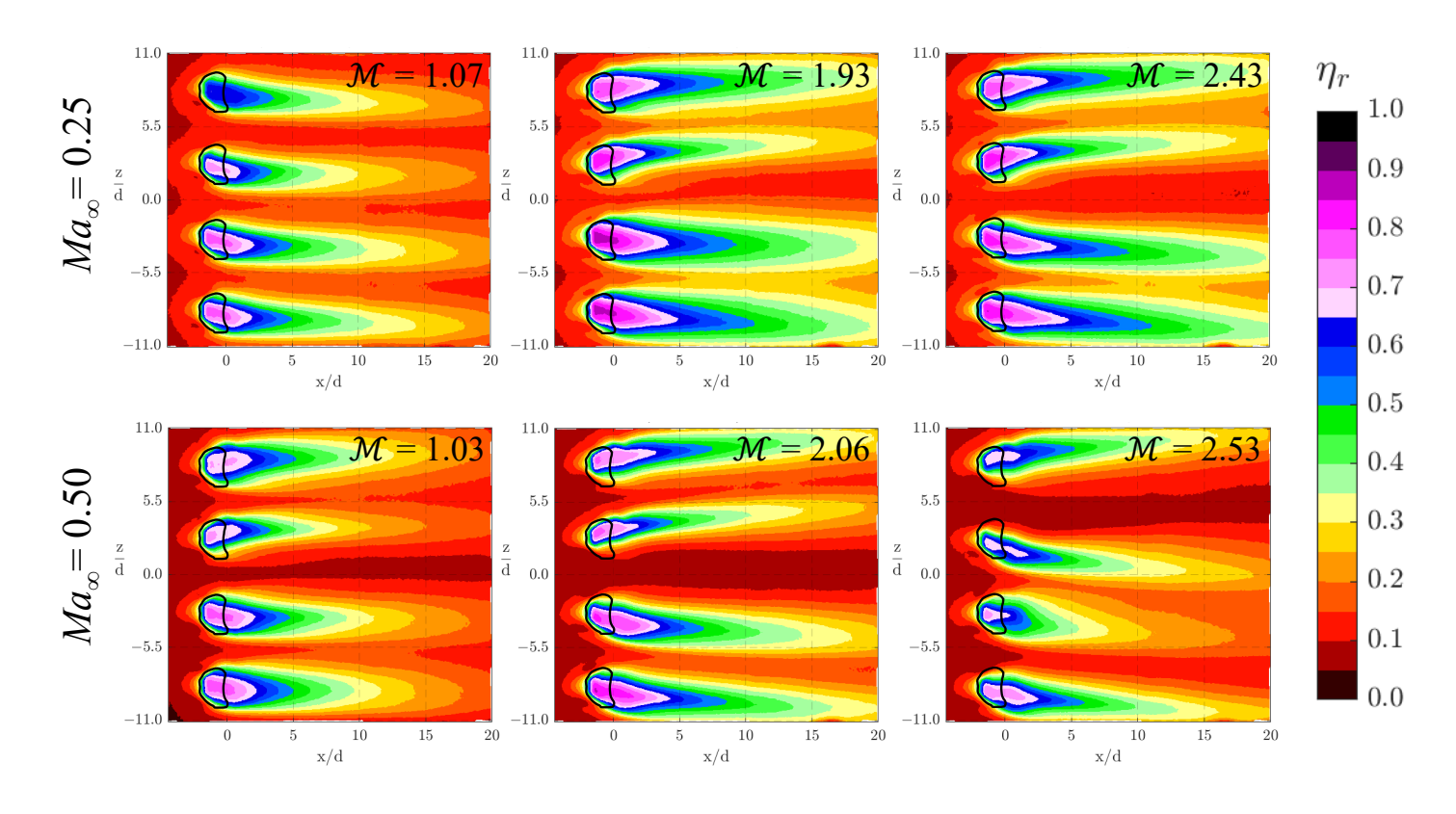


FIGURE 9: AOPT η_r DISTRIBUTION FOR Ma_{∞} = 0.25 AND 0.5, CONDUCTION CORRECTED

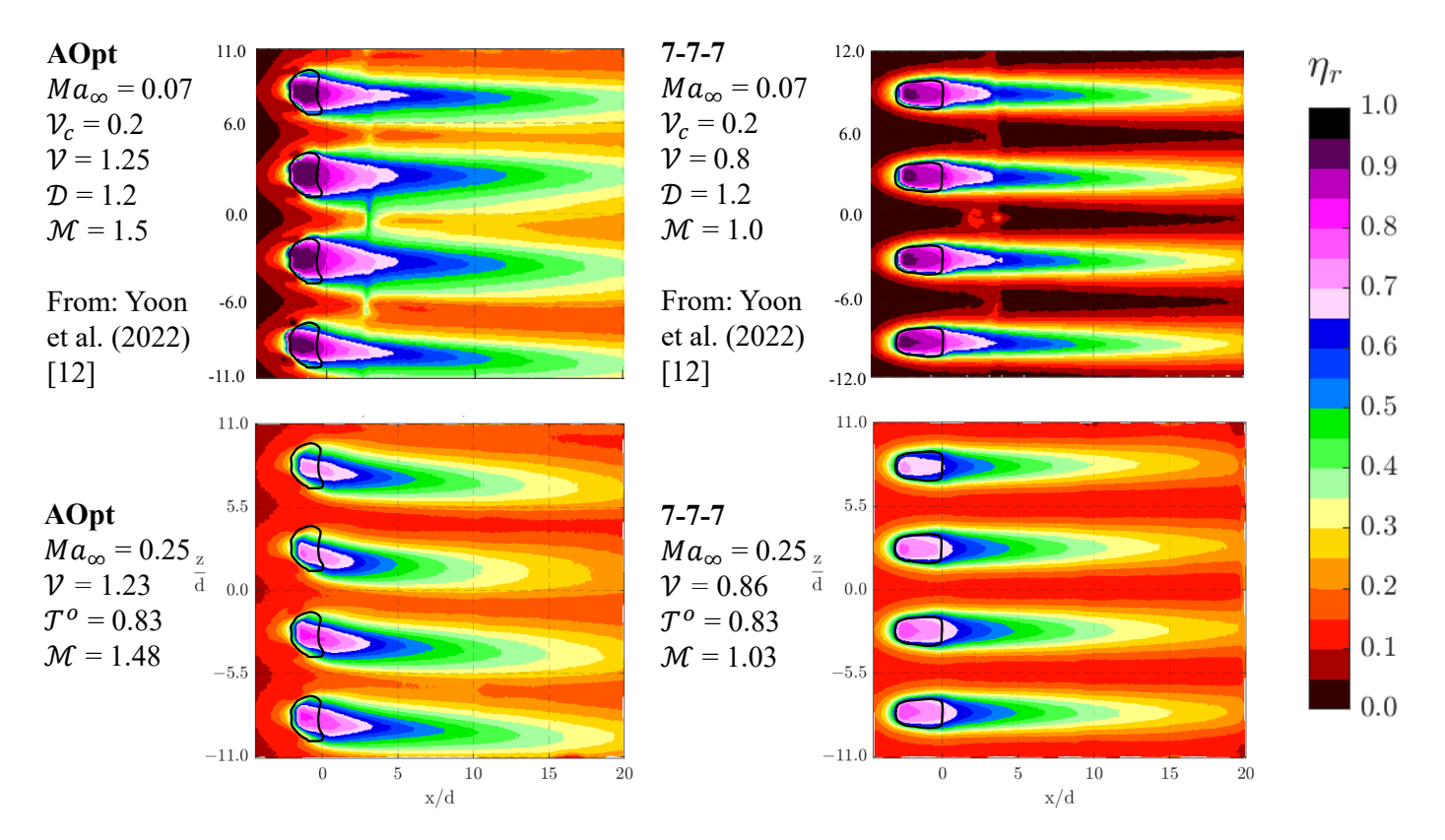


FIGURE 10: COMPARISON OF η CONTOURS FOR THE AOPT HOLES AND 7-7-7 HOLES TO LOW Ma RESULTS FROM YOON ET AL.[12]

CONCLUSIONS

This study is the first experimental paper done with a newly developed high speed wind tunnel facility at the University of Texas at Austin. A comparison was made between the effectiveness of two different film cooling hole geometries as the Mach number and blowing ratio were varied.

Despite the biasing of the jets observed in the contours of adiabatic effectiveness for the AOpt holes, the optimized geometry still outperformed the 7-7-7 hole at all blowing ratios when comparing data taken at the same mainstream Mach number. The large coverage of the hole more evenly spreads the coolant out across the surface even in the presence of jet biasing. However, this biasing contributed to reduced effectiveness levels relative to the baseline, incompressible studies performed previously.

When comparing the same hole geometries at different mainstream Mach number, a noticeable degradation in performance was observed for both the 7-7-7 and optimized geometry when the blowing ratio exceeded unity. Based on observation of the jet profiles for each case, it is plausible that augmented pressure ratios which accompany higher mainstream Mach number cause complex interactions within the film cooling hole. Flow features such as large separation regions and shocks may significantly impact performance.

While this demonstration of high speed measurements gave insight into the challenges compressible flow causes for film cooling, much future work needs to be done to improve both experimental capabilities and understanding of the flow characteristics. In addition to improving measurement quality, future work will

elaborate upon the findings of this study, evaluating a broader scope of flow conditions and higher mainstream Mach number. Accompanying the results of these new studies, new hole geometries will be developed to mitigate the poor performance due to high-Mach number effects.

ACKNOWLEDGMENTS

This paper is based upon work supported by the National Science Foundation GOALI program Award Number 1936676, and by the Department of Energy under Award Number DE-FE0025011. This report was prepared as an account of work sponsored by an agency of the United States Government. Neither the United States Government nor any agency thereof, nor any of their employees, makes any warranty, express or implied, or assumes any legal liability or responsibility for the accuracy, completeness, or usefulness of any information, apparatus, product, or process disclosed, or represents that its use would not infringe privately owned rights. Reference herein to any specific commercial product, process, or service by trade name, trademark, manufacturer, or otherwise does not necessarily constitute or imply its endorsement, recommendation, or favoring by the United States Government or any agency thereof. The views and opinions of authors expressed herein do not necessarily state or reflect those of the United States Government or any agency thereof.

Additionally, the authors would like to thank Jon Hahne and the staff of the Center for Electromechanics for their assistance in the construction of the wind tunnel facility.

REFERENCES

- [1] Bogard, David G and Thole, Karen A. "Gas turbine film cooling." *AIAA Journal of Propulsion and Power* Vol. 22 No. 2 (2006): pp. 249–270. DOI https://doi.org/10.2514/1.18034.
- [2] Jones, Fraser B., Oliver, Todd and Bogard, David G. "Adjoint Optimization of Film Cooling Hole Geometry." Volume 5A: Heat Transfer Combustors; Film Cooling: p. V05AT12A014. 2021. American Society of Mechanical Engineers, Virtual, Online. DOI 10.1115/GT2021-59332.
- [3] Liess, C. "Experimental Investigation of Film Cooling With Ejection From a Row of Holes for the Application to Gas Turbine Blades." *Journal of Engineering for Power* Vol. 97 No. 1 (1975): pp. 21–27. DOI 10.1115/1.3445904.
- [4] Zhou, Wenwu, Johnson, Blake and Hu, Hui. "Effects of Flow Compressibility and Density Ratio on Film Cooling Performance." *Journal of Propulsion and Power* Vol. 33 No. 4 (2017): pp. 964–974. DOI 10.2514/1.B36275.
- [5] Gritsch, M., Schulz, A. and Wittig, S. "Adiabatic Wall Effectiveness Measurements of Film-Cooling Holes With Expanded Exits." *Journal of Turbomachinery* Vol. 120 No. 3 (1998): pp. 549–556. DOI 10.1115/1.2841752.
- [6] Saumweber, Christian and Schulz, Achmed. "Free-Stream Effects on the Cooling Performance of Cylindrical and Fan-Shaped Cooling Holes." *Journal of Turbomachinery* Vol. 134 No. 6 (2012): p. 061007. DOI 10.1115/1.4006287.
- [7] Oliver, Todd A., Bogard, David G. and Moser, Robert D. "Large eddy simulation of compressible, shaped-hole film cooling." *International Journal of Heat and Mass Transfer* Vol. 140 (2019): pp. 498–517. DOI 10.1016/j.ijheatmasstransfer.2019.04.119.
- [8] Schroeder, Robert P. and Thole, Karen A. "Adiabatic Effectiveness Measurements for a Baseline Shaped Film Cooling Hole." *Volume 5B: Heat Transfer*: p. V05BT13A036. 2014. American Society of Mechanical Engineers, Düsseldorf, Germany. DOI 10.1115/GT2014-25992.
- [9] Fox, Dale W., Furgeson, Michael. and Bogard, David G. "Considerations for Compressible Film Cooling: A Com-

- putational Study of The Effects of Transonic Flows and Varying Mainstream Mach Number." *ASME Turbo Expo 2023: Turbomachinery Technical Conference and Exposition*. 2023. American Society of Mechanical Engineers.
- [10] Van Driest, E. R. "Turbulent Boundary Layer in Compressible Fluids." *Journal of the Aeronautical Sciences* Vol. 18 No. 3 (1951): pp. 145–160. DOI 10.2514/8.1895.
- [11] Gutierrez, Daniel, Yoon, Christopher, Furgeson, Michael T., Veley, Emma M., Bogard, David G. and Thole, Karen A. "Experimental Evaluation of Adjoint Based Optimized Film Cooling Holes - Part I: Baseline Adiabatic and Overall Cooling Effectiveness." *Proceedings of ASME Turbo Expo 2022*. 2022. Rotterdam, The Netherlands. DOI 10.1115/GT2022-83436.
- [12] Yoon, Christopher, Gutierrez, Daniel, Furgeson, Michael T. and Bogard, David G. "Evaluation of Adjoint Optimized Hole Part II: Parameter Effects on Performance." Volume 6A: Heat Transfer Combustors; Film Cooling: p. V06AT12A031. 2022. American Society of Mechanical Engineers, Rotterdam, Netherlands. DOI 10.1115/GT2022-82726.
- [13] "Guide to 3D Printing Tolerances, Accuracy, and Precision." Accessed 2023-02-18, URL https://formlabs.com/blog/understanding-accuracy-precision-tolerance-in-3d-printing/.
- [14] Gritsch, M, Schulz, A and Wittig, S. "Discharge coefficient measurements of film-cooling holes with expanded exits." *Journal of Turbomachinery* Vol. 120 No. 3 (1998): pp. 557–563. DOI 10.1115/1.2841753.
- [15] Moffat, R. J. "Using Uncertainty Analysis in the Planning of an Experiment." *Journal of Fluids Engineering* Vol. 107 No. 2 (1985): pp. 173–178. DOI 10.1115/1.3242452.
- [16] Anderson, Joshua B., Boyd, Emily J. and Bogard, David G. "Experimental Investigation of Coolant-to-Mainstream Scaling Parameters With Cylindrical and Shaped Film Cooling Holes." *Volume 5B: Heat Transfer*: p. V05BT12A033. 2015. American Society of Mechanical Engineers, Montreal, Quebec, Canada. DOI 10.1115/GT2015-43072.